MITSUBISHI ELECTRIC RESEARCH LABORATORIES
https://www.merl.com

High-Torque Direct-Drive Machine with Combined Axial- and Radial-flux Out-runner Vernier Permanent Magnet Motor

Zhou, Lei; Guo, Feng; Wang, Hongyu; Wang, Bingnan

TR2021-050 May 18, 2021

Abstract

This paper presents the design, modeling, and simulation for a novel type of high-torque motor, targeting various direct-drive applications, such as robotic actuator, precision motion rotatry stages, and in-wheel drive for electrical vehicles. The key idea of the motor design is to use a combination of (a) combined axial- and radial-flux electric machine and (b) Vernier permanent magnet (VPM) motor. Such combination effectively increases the torque generation capability for the proposed motor, and makes it attractive for direct-drive applications. Analytical model for the motor's performance is derived and is validated using finite element method (FEM), and is used for optimizing the motor design parameters. Motor's losses and efficiency are evaluated by finite element simulations for various magnetic material selections. The mechanical design for the motor is also discussed. The simulation result of the proposed motor demonstrates a 1.5x torque improvement compared with a baseline off-she-shelf direct-drive machine of the same size. The comparison shows that the proposed design is promising for the next-generation high-torque direct-drive motors.

IEEE International Electric Machine & Drives Conference (IEMDC)

Mitsubishi Electric Research Laboratories, Inc.
201 Broadway, Cambridge, Massachusetts 02139

High-Torque Direct-Drive Machine with Combined Axial- and Radial-flux Out-runner Vernier Permanent Magnet Motor

Lei Zhou*, Feng Guo†, Hongyu Wang‡ and Bingnan Wang §
*Department of Mechanical Engineering, The University of Texas at Austin, Austin, TX, USA.
†‡§ Mitsubishi Electric Research Laboratories, Cambridge, MA, USA
Email: *lzhou@utexas.edu, † fguo9@hawk.iit.edu, ‡ howang@merl.com, § bwang@merl.com

***Abstract*—This paper presents the design, modeling, and simulation for a novel type of high-torque motor, targeting various direct-drive applications, such as robotic actuator, precision motion rotatry stages, and in-wheel drive for electrical vehicles. The key idea of the motor design is to use a combination of (a) combined axial- and radial-flux electric machine and (b) Vernier permanent magnet (VPM) motor. Such combination effectively increases the torque generation capability for the proposed motor, and makes it attractive for direct-drive applications. Analytical model for the motor's performance is derived and is validated using finite element method (FEM), and is used for optimizing the motor design parameters. Motor's losses and efficiency are evaluated by finite element simulations for various magnetic material selections. The mechanical design for the motor is also discussed. The simulation result of the proposed motor demonstrates a 1.5× torque improvement compared with a baseline off-she-shelf direct-drive machine of the same size. The comparison shows that the proposed design is promising for the next-generation high-torque direct-drive motors.**

***Index Terms*—Vernier Permanent magnet Motor, Direct-Drive Motor, Axial Flux Machine**

I. Introduction

In recent years, direct-drive machines are receiving increasing research attention due to their fast-growing need in emerging application areas, such as precision positioning stages in machine tools, robots, and in-wheel drives for electric vehicles. Direct-drive motors have many advantages: (a) The elimination of transmission mechanism, such as gearboxes, can effectively reduce the volume of the actuator assembly, which enables a much more compact system; (b) gearbox fault is one of the major failure modes for geared motors; the direct-drive motors eliminates the transmission and effectively improve the system's reliability; (c) transmission mechanisms such as gearboxes typically have nonlinear dynamics such as backlash hysteresis and nonlinear Coulomb friction, which can impair the system's dynamic performance and thus is not favorable for precision applications; the use of direct-drive machines can significantly improve the system's dynamic performance, which is important for position servo applications; (d) the elimination of transmission mechanism can improve the system's efficiency. These facts motivated a series of innovations in motor technology in order to realize motors for direct-drive applications.

Direct-drive machines need to have high specific torque (torque-to-weight ratio), torque density (torque-to-volume ratio), relatively high efficiency at low speed operation, and a compact form factor. Through the years, a number of research and development efforts have created various motor topology innovations aiming at pushing the torque density and specific torque limits for motors. Most studies for direct-drive motors have been mainly focusing on surface-mount permanent magnet (PM) synchronous motors, since they are known for their high torque generation capability among various motor types. References [1], [2] have reported various axial-flux PM motor designs with high torque density targeting at direct-drive applications, which allow reduced shaft-length without losing the motor's air gap area. In order to increase the effective torque generation area over the rotor's surface, multi-stage motors [3], [4] and combined axial- and radial-flux motors [5], [6] are studied. In these designs, the torque-generating air gap area are distributed over the rotor's surface. With approximately constant shear stress generation in all air gaps, such designs can effectively improve the motor's torque capability. Another method to increase the motor's torque capability is through increasing the motor's pole pair number, as discussed in references [7], [8]. With the same motor size and power, increasing the motor's pole pair number can increase the motor's torque while reducing the motor's output speed, and therefore making the motor more suitable for direct-drive applications. In recent years, the VPM motor is receiving drastically increasing research attention for high-toque, low-speed application, and references [9]–[12] report analysis and various designs for VPM motors. A VPM motor can be viewed as a combination of a magnetic gear and a regular PM motor, and therefore can deliver improved torque capability. Such motor configuration has shown promise for the next-generation direct-drive machines for various applications.

This paper describes a new design of high-torque direct-drive motor as shown in Fig. 1. The motor has an out-runner configuration, with the stator assembly in the center and the rotor surrounding the stator. The motor

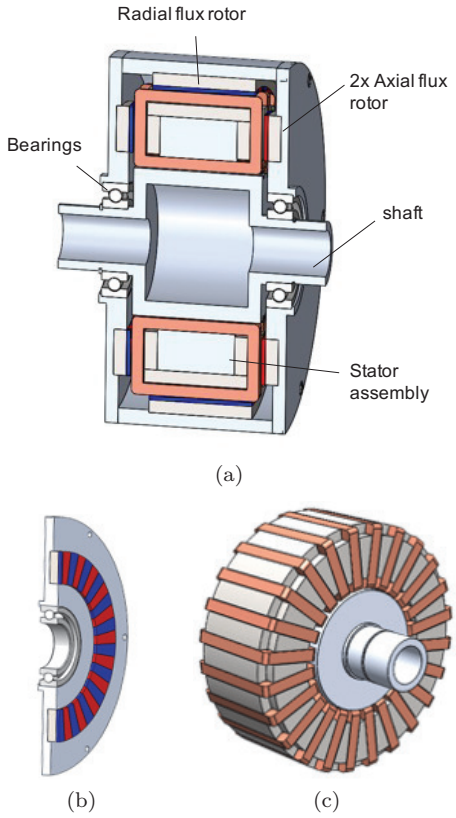

Fig. 1. CAD design for the proposed machine. (a) Cross-section view of motor assembly. (b) Axial-flux rotor. (c) Stator assembly.

uses combined axial- and radial-flux for torque generation, which effectively increases the shear stress generation area over the rotor's surface, and thus improve the motor's torque capability. The stator assembly has three stator yoke segments made of electric laminations, two for axial-flux motors and one for radial-flux motor. Toroidal windings are configured in the slots for all stator segments, which effectively reduces the end-turn length for the machine and thus beneficial for efficiency. Finally VPM motor principle is used for both axial- and radial-flux motors to further improve the torque generation using the magnetic gearing effect. The vision is that such new motor design can significantly out-perform the existing direct-drive machines in terms of torque capability, and thus benefit various direct-drive applications. Simulation shows that the proposed motor configuration can provide 1.5× improved torque comparing with an off-the-shelf direct-drive motor of the same size.

The rest of this paper is organized as follows. Section II briefly describes the operating principle, analytical modeling, and numerical validation for VPM motors. Section III presents the design parameter selections and motor performance scaling with respect to the motor sizing based on the model. Section IV discusses the material selection and mechanical design for the proposed motor. Section V presents a performance comparison between the proposed

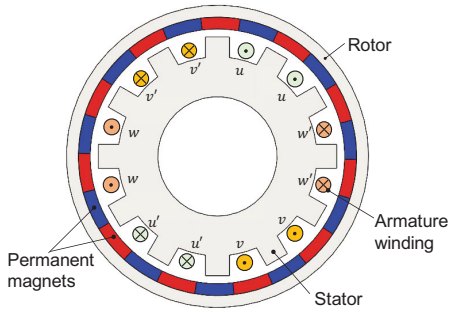

Fig. 2. Diagram of an out-runner vernier permanent magnet motor.

motor design and an off-the-shelf direct drive motor. The conclusion and future work is presented in Section VI.

II. Operating Principle and Modeling for VPM Motors

This section briefly presents the operating principle and modeling method for radial and axial VPM motors to make this paper self-contained. Figure 2 shows a diagram for a VPM motor. Here, the stator yoke has a toothed-pole structure, with motor windings configured in the slots, and the rotor has surface-mount PMs. The stator yoke and the rotor back-iron are made of electric laminations.

The rest of this section presents an analytical model for both radial and axial flux VPM motors. The assumptions of our models include: (a) Magnetic reluctance and saturation of steel parts are neglected; (b) the air gap length is small compared with the motor's radius; the flux density, magnetomotive force (MMF), and air gap permeance vary only in the circumference direction, and are uniform in the radial direction; (c) only fundamental harmonic of magnet MMF is considered.

A. Radial-Flux VPM Motor Modeling

We first describes the analytical model for a radial-flux VPM motor's torque generation. In a VPM motor, the fundamental-harmonic of MMF generated by the PMs on the rotor is

$$\mathcal{F}_{pm}(\theta_s) \approx \mathcal{F}_{pm_1} \cos\left(Z_r\theta_s - Z_r\omega_r t\right), \tag{1}$$

where $\mathcal{F}_{pm_1} = \frac{4}{\pi}\frac{B_r h_m}{\mu_0}$, Z_r is the magnet array's number of pole-pairs, θ_s is the angular coordinate in the stator-fixed frame, θ_m is the rotor's angular position, μ_0 is the vacuum permeability, h_m is the magnet thickness, and B_r is the remanence of the permanent magnet. Considering the average and fundamental-harmonic air gap permeance, the air gap permeance can be approximated by

$$P_g(\theta_s) \approx P_0 + P_1\cos(Z_s\theta_s), \tag{2}$$

where

$$P_0 = \frac{\mu_0}{g'}\big(1 - 1.6\beta\frac{b_0}{t}\big),$$
$$P_1 = \frac{\mu_0}{g'}\frac{4}{\pi}\beta\big(\frac{1}{2} + \frac{(b_0/t)^2}{0.78125 - 2(b_0/t)^2}\big)\sin\left(1.6\pi\frac{b_0}{t}\right)$$
$$\beta = 0.5 - \frac{1}{2\big(1 + (b_0/2g')^{-\frac{1}{2}}\big)},$$

Z_s is the stator teeth number, b_0 is the slot opening, t is the slot pitch, g is the mechanical air gap length, and $g' = g + h_m$ is the magnetic air gap length. Then the air gap flux density generated by the PMs is

$$\begin{aligned} B_{pm} =& \mathcal{F}_{pm}(\theta_s)P_g(\theta_s) \\ \approx& \mathcal{F}_{pm_1}\cos\big(Z_r(\theta_s - \theta_m)\big)\big(P_0 + P_1\cos(Z_s\theta_s)\big) \\ =& B_{pm_1}\cos((Z_r \pm Z_s)\theta_s - Z_r\theta_m) \\ &+ B_{pm_h}\cos(Z_r(\theta_s - \theta_m)), \end{aligned} \tag{3}$$

where $B_{pm_1} = \frac{\mathcal{F}_{pm_1}P_1}{2}$, and $B_{pm_h} = \mathcal{F}_{pm_1}P_0$

Considering only the fundamental and slot harmonics, the stator winding distribution in one phase is

$$\begin{aligned} N_s(\theta_s) \approx& \frac{4}{\pi}k_w\big(N\cos(p\theta_s) + N_{h1}\cos((Z_s - p)\theta_s) \\ &- N_{h2}\cos((Z_s + p)\theta_s)\big), \end{aligned} \tag{4}$$

where N is the number of turns of stator windings per phase per pole, and k_w is the winding factor, Z_s is the number of stator teeth, N_{h1} and N_{h2} are the magnitude of the teeth harmonics in the stator winding distribution. For concentrated full-pitch windings, we have $N_{h1} = N/(Z_s/p - 1)$, and $N_{h2} = N/(Z_s/p + 1)$. Then the flux linkage in one phase of winding due to the PM-generated flux is

$$\lambda_s(\theta_s) = lR\int_0^{2\pi} N_s(\theta_s)B_{pm}(\theta_s)\mathrm{d}\theta_s, \tag{5}$$

where R and l are the rotor radius and axial length, respectively.

For VPM motors we have $Z_r = Z_s \pm p$. Assume $Z_r = Z_s - p$, then (5) yields

$$\lambda_s(\theta_s) = 4Rlk_w(NB_{pm_1} + N_{h1}B_{pm_h})\cos(Z_r\theta_m). \tag{6}$$

Assume $N_{h1} = N/(Z_s/p - 1)$. With sinusoidal currents of magnitude I_s in the three-phase windings, the motor's torque is

$$T_e = 6Z_rRlk_wN(B_{pm_1} + \frac{B_{pm_h}}{Z_r/p})I_s. \tag{7}$$

B. Axial-Flux VPM Motor Modeling

Next we present the modeling for torque generation of an axial-flux VPM motor, and discuss the difference between the radial flux and axial flux motor. This derivation is largely based on reference [**?**].

The major difference between a radial- and axial-flux motor is that the axial motor's geometry, fields, and torques depend on the radius r. In an axial-flux vernier motor, the fundamental harmonic of the rotor MMF is

$$\mathcal{F}^a_{pm}(\theta_s) = \mathcal{F}^a_{pm_1}\cos\big(Z_r\theta_s - Z_r\omega_r t\big), \tag{8}$$

where

$$\mathcal{F}_{pm_n} = \frac{4}{n\pi}\frac{B_r h_m}{\mu_0}. \tag{9}$$

The axial flux motor's air gap permeance is

$$P^a_g(\theta_s) \approx P^a_0(r) + P^a_1(r)\cos(Z_s\theta_s), \tag{10}$$

where

$$P^a_0(r) = \frac{\mu_0}{g'^a}\big(1 - 1.6\beta\frac{b_0(r)}{t(r)}\big), \tag{11}$$
$$g'^a = g^a + h_{mag}, \tag{12}$$
$$P^a_1(r) = \frac{\mu_0}{g'^a}\frac{4}{\pi}\beta\big(\frac{1}{2} + \frac{(\frac{b_0}{t(r)})^2}{0.78 - 2(\frac{b_0}{t(r)})^2}\big)\sin\left(1.6\pi\frac{b_0(r)}{t(r)}\right), \tag{13}$$
$$\beta = 0.5 - \frac{1}{2\big(1 + (b_0(r)/2g')^{-\frac{1}{2}}\big)}. \tag{14}$$

Note that in an axial-flux machine the slot opening b_0 and slot pitch t are both functions of the radius r. Assume that the axial-flux motor has constant slot opening b_0. Then the PM-generated air gap flux for the axial-flux vernier PM motor is

$$\begin{aligned} B^a_{pm}(\theta_s, r) =& \mathcal{F}^a_{pm}(\theta_s)P^a_g(\theta_s) \\ \approx& \mathcal{F}_{pm_1}\cos\big(Z_r(\theta_s - \theta_m)\big)\big(P^a_0(r) + P^a_1(r)\cos(Z_s\theta_s)\big) \\ =& \mathcal{F}_{pm_1}P^a_0(r)\cos(Z_r(\theta_s - \theta_m)) \\ &+ \frac{\mathcal{F}_{pm_1}P^a_1(r)}{2}\cos((Z_r - Z_s)\theta_s - Z_r\theta_m) \\ &+ \frac{\mathcal{F}_{pm_1}P^a_1(r)}{2}\cos((Z_r + Z_s)\theta_s - Z_r\theta_m). \end{aligned} \tag{15}$$

Considering the stator winding distribution

$$\begin{aligned} N^a_s(\theta_s) \approx& \frac{1}{2}k^a_w\frac{4}{\pi}\big(N\cos(p\theta_s) + N_{h1}\cos((Z_s - p)\theta_s) \\ &+ N_{h2}\cos((Z_s + p)\theta_s)\big), \end{aligned} \tag{16}$$

where N is the number of winding per phase per pole, $N_{h1} = N/(Z_s/p - 1)$, $N_{h2} = N/(Z_s/p + 1)$.

Selecting $Z_r = Z_s - p$, then we have $N_{h1} = N/(Z_r/p)$. The stator winding's flux linkage can be calculated as

$$\begin{aligned} \lambda^a_s(\theta_s) =& \int_{kD_o/2}^{D_o/2}\left(\int_0^{2\pi} N^a_s(\theta_s)B^a_{pm}(\theta_s, r)\mathrm{d}\theta_s\right)r\mathrm{d}r \\ =& \frac{2}{\pi}\mathcal{F}^a_{pm_1}k^a_w N\cos(Z_r\theta_m)(\frac{f_{P_0}}{Z_r/p} \pm f_{P_1}), \end{aligned} \tag{17}$$

where

$$f_{P_0} = \int_{kD_o/2}^{D_o/2} P^a_0(r)r\mathrm{d}r = \frac{\mu_0}{8g'^a}D_o^2(1 - k^2)(1 - \frac{1.6\beta b_0}{t_{avg}}), \tag{18}$$

$$f_{P_1} = \int_{kD_o/2}^{D_o/2}\frac{P^a_1(r)}{2}r\mathrm{d}r. \tag{19}$$

Selecting $Z_r = Z_s - p$, the back-emf in the stator winding

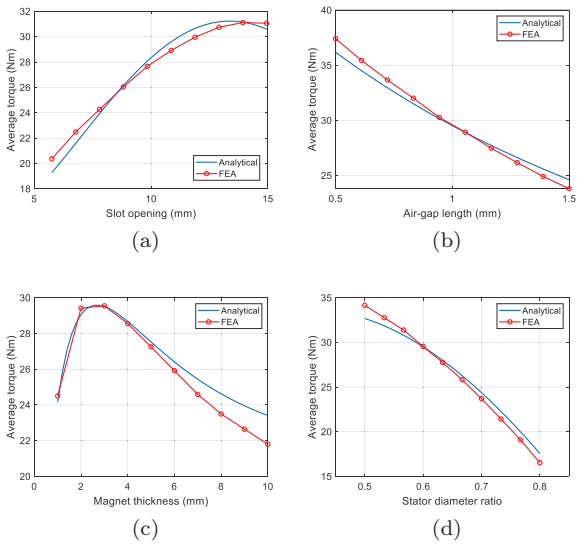

Fig. 3. Comparison between analytically-modeled VPM motor torque and FEM simulation results while sweeping key design parameters. (a) Slot opening length. (b) Air gap length, (c) Magnet thickness. (d) Inner diameter and outer diameter ratio for axial-flux VPM motor.

is

$$e = -\frac{\mathrm{d}}{\mathrm{d}t}\lambda_s = \frac{2}{\pi}\mathcal{F}^a_{pm_1} k^a_w N Z_r \omega_r \left(\frac{f_{P_0}}{Z_r/p} \pm f_{P_1}\right) \sin(Z_r \omega_r t). \tag{20}$$

Then the generated torque of the axial motor can be calculated as

$$T_{axial} = \frac{3}{\pi}\mathcal{F}^a_{pm_1} k^a_w N Z_r I_s \left(\frac{f_{P_0}}{Z_r/p} + f_{P_1}\right). \tag{21}$$

C. Model Validation

The analytical models for radial- and axial-flux VPM motors are validated using numerical simulations. Figure 3 shows the comparison between the analytically calculated combined VPM motor's torque generation and finite element simulation results as a function of several key design parameters. Note that this simulation is only for model validation, and the design choice of the parameters do not reflect the parameter selection for the proposed machine. The good agreement of the results validates the developed analytical model.

III. Design parameter selection

This section discusses the design parameter selection for the proposed motor. Here the validated analytical models are used for motor performance prediction. The design parameters include two groups: The first group of parameters is the detailed motor design geometrical parameters that can scale with the motor size, such as slot opening width, magnet thickness, air gap length, rotor back-iron thickness, etc. The second group is the motor's overall sizing parameters, including the motor outer diameter, axial length, and the ratio between inner and outer diameter for the axial-flux machine.

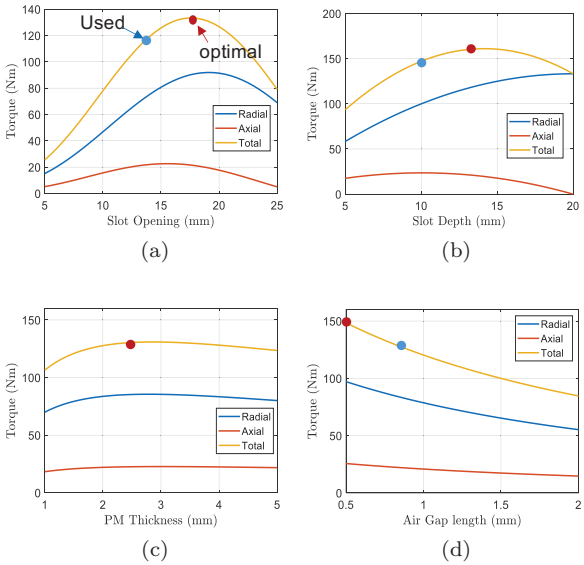

Fig. 4. Detailed motor design parameter selection for motor design.

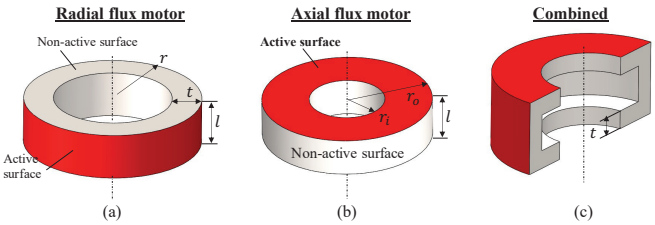

Fig. 5. Diagrams of motor topology comparison. Red surfaces: active (torque-generation) surfaces. Grey surfaces: non-active surfaces. (a) Radial-flux machine. (b) Axial-flux machine. (c) Combined axial- and radial-flux machine.

We first present the detailed design parameter selections. These selections are based on the simulation results using the analytical motor model created in Section II. Figure 4 shows the motor's torque performance with respect to various design parameters, where the red dots show the optimal value for torque generation. However, sub-optimal design parameters indicated by the blue dots in Fig. 4 are selected for the motor due to manufacturing feasibility.

We next discuss the overall motor sizing selection for the proposed motor topology. Figure 5 shows the diagram of rotors for radial-flux, axial-flux, and combined radial- and axial-flux electric machines, where the red surfaces are the active torque-generating surfaces of the rotor. Assume a constant shear stress generation τ_e on the rotor's active surfaces. For the machine configurations shown in Fig. 5, the scaling of the motor's torque, mass, volume, specific torque, and torque density are shown in Table I, where l is the rotor's axial length, r is the air gap radius of the radial-flux motor, r_o and r_i are the outer and inner air gap radius of the axial-flux machine, respectively, ρ is the motor's density, and t is the thickness of the radial-flux motor ring with the stator thickness considered. Table I

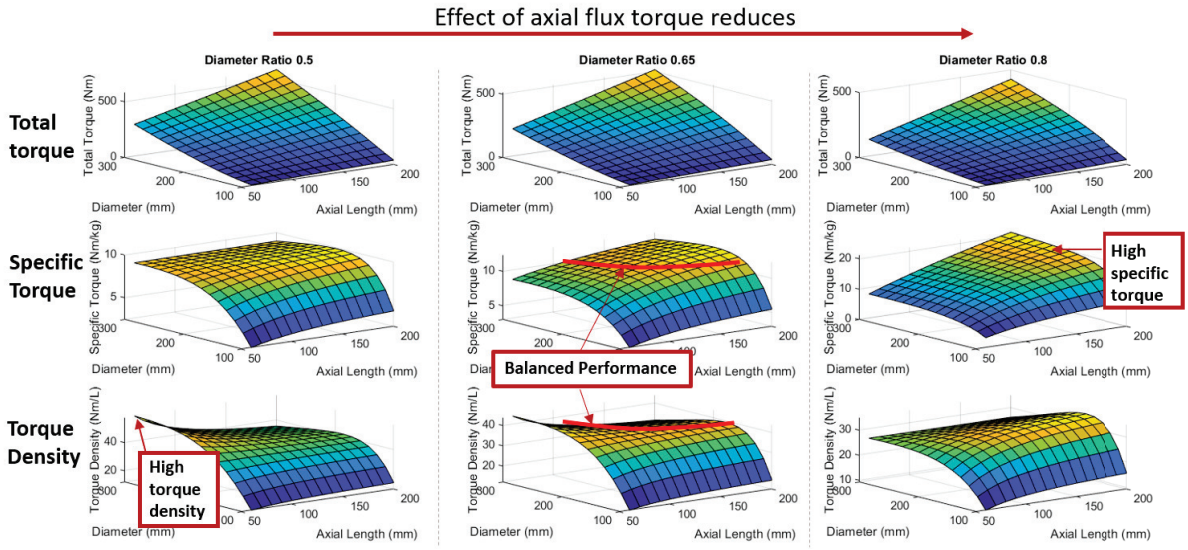

Fig. 6. Motor overall sizing design selections.

TABLE I
SCALING OF PERFORMANCE WITH OVERALL DIMENSIONS.

Spec	Radial Flux	Axial flux	Combined
Torque T	$2\pi r^2 l\tau_e$	$\frac{2\pi}{3}(r_o^3 - r_i^3)\tau_e$	$A_1T_r + A_2T_a$
Mass m	$2\pi\rho rtl$	$\pi\rho l(r_0^2 - r_i^2)$	$A_1m_r + A_2m_a$
Volume V	$\pi r^2 l$	$\pi r_o^2 l$	$A_1V_r + A_2V_a$
T/m	$r^2 l/t$	r_o^3	$A_1r^2l + A_2r_o^3$
T/V	r	r_o/l	$A_1 + A_2r/l$

shows that the radial flux motor performs best when the machine has large radius and low motor ring thickness, while the axial motor performs best when the machine has small axial length. However, for general sized motors, radial or axial flux machine alone cannot provide good overall performance.

This paper proposes a motor design that uses a combination of radial- and axial-flux for torque generation as shown in Fig. 5, and uses toroidal winding for the stator. This design effectively utilize the end turns and thus further improve the torque capability of a pure radial- or axial-flux electric machine. Moreover, from Table I, one can find that using a combination of both axial- and radial-flux machines can produce balanced performance between torque density and specific torque, and thus allow machine design optimized for a specific application.

Figure 6 shows the simulated total torque [N·m], specific torque [N·m/kg], and torque density [N·m/L] for the proposed motor design while sweeping of the motor's outer diameter length and axial length under different ratio of inner diameter and outer diameter. Here a magnetic gear ratio of $Z_r = 22$ is selected. With a larger diameter ratio, the contribution of the axial-flux motor to the total torque generation reduces. The result shown in Fig. 6 allows us to make design selection for various target applications. For example, for robotic applications where the specific torque is important, one can design motor with large diameter ratio and large diameter. For volume-constraint applications where the torque density should be optimized, the motor should have large motor diameter, small axial length, and small diameter ratio to fully utilize the axial-flux motor torque generation. Various design choices in between provide balanced performance of specific torque and torque density for different applications.

IV. Material Selection and Mechanical Design

This section discusses the material selections and mechanical design considerations for the proposed motor. Due to the three-dimensional distribution of the magnetic flux, we consider both soft magnetic composite (SMC) and electric laminations for the stator yoke and rotor back-iron materials. Table II shows a comparison between the properties of electrical laminations and SMC materials from Hoganas Inc. It can be observed that compared with electric laminations, the SMC materials have significantly smaller magnetic permeability and larger coercivity, which can impair the motor's performance. Therefore in this work, we select electric laminations for the stator and rotor back-iron materials.

The electric lamination material needs to be oriented in the proper direction to prevent excessive eddy current loss. This prevents us from using a single piece for the stator yoke in both axial- and radial-flux motors. Figure 7 shows the proposed stator assembly's mechanical design. Here the stator yoke is made of three different parts: two axial-flux stator yokes made of spiral electric laminations, and one radial-flux stator yoke made of stacked laminations. The yokes are assembled to a non-magnetic core first, and the winding coils are configured in the slots wrapping all stator yoke segments. This design allows us to build the

TABLE II
PROPERTIES OF ELECTRICAL LAMINATION AND SOFT MAGNETIC COMPOSITE MATERIALS.

Material	μ_r	H_c	Resistivity	Density	Yield Strength	E
M19 Electric Steel	8000	56 A/m	0.05 $\mu\Omega$m (bulk)	7650 kg/m^3	358 MPa	150 GPa
SMC #1: Somaloy 1000 3P	950	217 A/m	70 $\mu\Omega$m	7560 kg/m^3	70 MPa	170 GPa
SMC #2: Somaloy 130i 5P	350	152 A/m	20000 $\mu\Omega$m	7440 kg/m^3	35 MPa	110 GPa

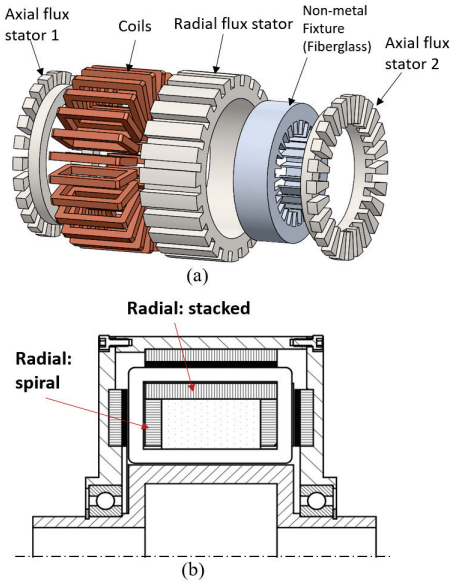

Fig. 7. Mechanical design of stator assembly. (a) Explode view of stator assembly. (b) Cross-section view of the full motor assembly showing lamination directions.

TABLE III
FEM SIMULATED MOTOR LOSS FOR PROPOSED MOTOR.

PM material	Current density [A/mm2]	Rotor speed [rps]	PM loss [W]	Core Hyst Loss [W]	Core eddy loss [W]	Copper Loss [W]	Efficiency
Solid	5	2	56.5	17.5	11.5	47	83%
Solid	10	2	150	28	24	188	76%
Solid	5	5	300	45	50	47	80%
Solid	10	5	835	60	100	188	74%
Laminated	5	2	10	5	8	47	91%
Laminated	10	2	19	26	12	188	86%
Laminated	5	5	43	40	31	47	91%
Laminated	10	5	105	58	73	188	89%

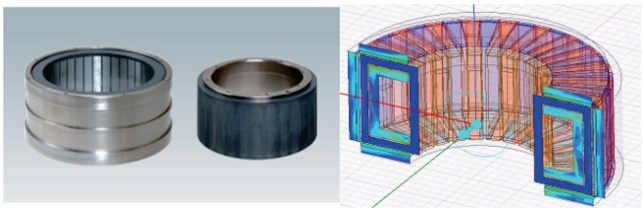

(a) (b)

Fig. 8. (a) Baseline direct-drive motor Mitsubishi Electric TM-RBP150G20. (b) Simulated field distribution of the proposed machine.

combined axial- and radial-flux machine with stator yoke made of electric laminations.

One of the major limitation of VPM machine is the relatively high eddy current losses in the PM. Laminating the magnets provides an effective solution to this challenge. One possible vendor for such laminated rare-earth permanent magnets is [13]. This design choise, however, will increase the motor's cost. Table III shows the FEM-simulated losses and efficiency of the proposed motor under solid and laminated permanent magnets, different current densities, and mechanical speed. It can be observed that the loss in the PM is drastically reduced when the motor is using laminated magnets, and the machine's efficiency is about 90%. When using solid magnets, the machine's efficiency is around 80%, which is also acceptable for direct-drive machines. Under this design, the machine should be operating at low speed (below 2 rps) to regulate the temperature of the magnets.

V. PERFORMANCE EVALUATION

The expected performance of the proposed motor design is compared with an off-the-shelf direct-drive motor. Here Mitsubishi Electric TM-RBP150G20 direct-drive motor with water cooling is selected as a benchmark, as shown in Fig. 8. Table IV shows the comparison of performance between the benchmark machine and the proposed motor with 22 rotor pole pairs and 34 rotor pole pairs. The three machines have the same overall dimensions. The expected performance of the motor is simulated using Ansys Maxwell under a current density of 10 A/mm^2. It can be observed in Table IV that the proposed motor design has more than 1.5 times torque improvement compared with the benchmark motor, and is able to deliver a high efficiency of about 90%. This comparison demonstrates the good potential of the proposed motor configuration for the development of high-torque direct-drive actuators.

VI. CONCLUSION AND FUTURE WORK

In this paper, we presented the design, modeling, and expected performance for a new type of high-torque direct-drive motor using combined axial- and radial-flux VPM motors. Analytical models for the motor's torque generation have been developed and validated by finite element simulations. The sizing and key parameter selection were

TABLE IV
PERFORMANCE COMPARISON BETWEEN THE PROPOSED MOTOR AND BENCHMARK MOTOR.

Specification	Mitsubishi Electric TM-RBP150G20	New motor I: 22 pole-pair	New motor II: 34 pole-pair
Outer diameter	230 mm	230 mm	230 mm
Axial length	130 mm	130 mm	130 mm
Continuous torque	150 Nm	**233 Nm (1.5×)**	**310 Nm (2×)**
Efficiency	–	**91%**	**88%**
Active mass	25 kg	**22.7 kg (10% ↓)**	**22.7 kg (10% ↓)**
Specific torque	6 Nm/kg	**9.91 Nm/kg (1.65×)**	**13.6 Nm/kg (2.28×)**
Torque density	27.7 Nm/L	**41.6 Nm/L (1.5×)**	**57.8 Nm/L (2×)**

conducted with the developed analytical model. New mechanical design was proposed for the stator assembly of the combined-flux motor. The simulated performance of the proposed motor demonstrated more than 1.5× torque improvement compared with off-the-shelf direct-drive machines. We are currently working on further optimization of the motor for reduced torque ripple and thermal design of the machine, and will work on the prototype construction and experimental evaluations in the future.

REFERENCES

[1] R. L. Ficheux, F. Caricchi, F. Crescimbini, and O. Honorati, "Axial-flux permanent-magnet motor for direct-drive elevator systems without machine room," *IEEE Transactions on Industry Applications*, vol. 37, no. 6, pp. 1693–1701, 2001.

[2] D. Moreels and P. Leijnen, "High efficiency axial flux machines," *MAGNAX White Paper*, vol. 1, 2018.

[3] F. Caricchi, F. Crescimbini, F. Mezzetti, and E. Santini, "Multistage axial-flux pm machine for wheel direct drive," *IEEE Transactions on Industry Applications*, vol. 32, no. 4, pp. 882–888, 1996.

[4] F. E. Hunstable, "Brushless electric motor/generator," May 21 2015, uS Patent App. 14/608,232.

[5] M. Namba, K. Hiramoto, and H. Nakai, "Variable-field machine with three-dimensional magnetic circuit for traction motor," in *2016 19th International Conference on Electrical Machines and Systems (ICEMS)*. IEEE, 2016, pp. 1–6.

[6] F. E. Hunstable, "Brushless electric motor/generator," Apr. 16 2019, uS Patent 10,263,480.

[7] J. Hollerbach, I. Hunter, J. Lang, S. Umans, R. Sepe, E. Vaaler, and I. Garabieta, "The mcgill/mit direct drive motor project," in *[1993] Proceedings IEEE International Conference on Robotics and Automation*. IEEE, 1993, pp. 611–617.

[8] M. G. Simões and P. Vieira, "A high-torque low-speed multiphase brushless machine-a perspective application for electric vehicles," *IEEE Transactions on Industrial Electronics*, vol. 49, no. 5, pp. 1154–1164, 2002.

[9] A. Ishizaki, T. Tanaka, K. Takasaki, and S. Nishikata, "Theory and optimum design of pm vernier motor," 1995.

[10] B. Kim and T. A. Lipo, "Operation and design principles of a pm vernier motor," in *2013 IEEE Energy Conversion Congress and Exposition*. IEEE, 2013, pp. 5034–5041.

[11] ——, "Analysis of a pm vernier motor with spoke structure," *IEEE Transactions on Industry Applications*, vol. 52, no. 1, pp. 217–225, 2015.

[12] D. Li, R. Qu, J. Li, L. Xiao, L. Wu, and W. Xu, "Analysis of torque capability and quality in vernier permanent-magnet machines," *IEEE transactions on industry applications*, vol. 52, no. 1, pp. 125–135, 2015.

[13] *L Type Laminated Magnet Datasheet*, Arnold Magnetic Technologies, 10 2020, rev. 1.1.